Title
New Particle Formation from Methanesulfonic Acid and Amines/Ammonia as a Function of Temperature

Journal
Environmental Science and Technology, 51(1)

ISSN
0013-936X

Authors
Chen, Haihan
Finlayson-Pitts, Barbara J

Publication Date
2017-01-03

DOI
10.1021/acs.est.6b04173

Peer reviewed

Environmental Science & Technology

Article

pubs.acs.org/est

New Particle Formation from Methanesulfonic Acid and Amines/Ammonia as a Function of Temperature

Haihan Chen and Barbara J. Finlayson-Pitts*

Department of Chemistry, University of California, Irvine, Irvine, California 92697, United States

Supporting Information

ABSTRACT: Previous studies have shown that methanesulfonic acid (MSA) reacts with amines and ammonia to form particles, which is expected to be particularly important in coastal and agricultural areas. We present the first systematic study of temperature dependence of particle formation from the reactions of MSA with trimethylamine (TMA), dimethylamine (DMA), methylamine (MA), and ammonia over the range of 21−28 °C and 0.4−5.9 s in a flow reactor under dry conditions and in the presence of 3×10^{17} cm^{-3} water vapor. Overall activation energies ($E_{overall}$) for particle formation calculated from the dependence of rates of particle formation on temperature for all of these bases are negative. The negative $E_{overall}$ is interpreted in terms of reverse reactions that decompose intermediate clusters in competition with the forward reactions that grow the clusters into particles. The average values of $E_{overall}$ for the formation of detectable particles are: TMA, −(168 ± 19) kcal mol^{-1}; DMA, −(134 ± 30) kcal mol^{-1}; MA, −(68 ± 23) kcal mol^{-1}; NH_3, −(110 ± 16) kcal mol^{-1} (±1σ). The strong inverse dependence of particle formation with temperature suggests that particle formation may not decline proportionally with concentrations of MSA and amines if temperature also decreases, for example at higher altitudes or in winter.

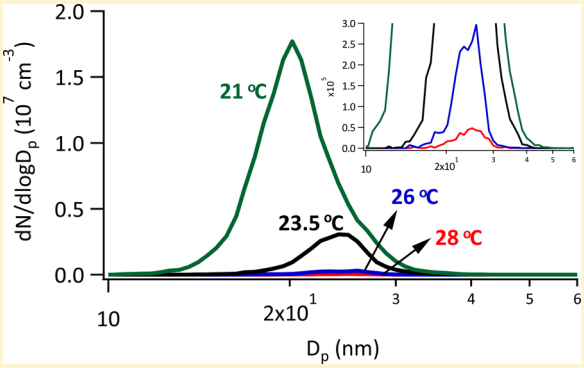

INTRODUCTION

New particle formation (NPF) from gas phase precursors is an important source of atmospheric particles.[1−4] It also contributes significantly to cloud condensation nuclei (CCN), which influence radiative forcing by changing cloud coverage and properties.[5−9] The species and mechanisms involved in NPF need to be well understood to quantitatively predict the impacts on visibility, human health, and climate.[1,10,11] While new particle formation events have been often observed to be associated with sulfuric acid (H_2SO_4),[12−21] other acids such as methanesulfonic acid (MSA, CH_3SO_3H) have also been suggested to contribute.[22−30]

Atmospheric MSA as well as SO_2 (the precursor to H_2SO_4) are formed from the oxidation of organosulfur compounds that originate in biological processes, agricultural activities, industrial operations, and biomass burning.[31−35] The major anthropogenic source of SO_2 (and hence H_2SO_4) in the troposphere is combustion of sulfur-containing fossil fuels. Particle formation from MSA could be comparable to that from H_2SO_4 in relatively clean coastal and ocean areas where the concentrations of atmospheric gas phase MSA are in the range of 10^5−10^7 molecules cm^{-3}, which is typically ∼10−100% of that of H_2SO_4.[36−40] In a recent study,[41] it was shown that while the gas phase concentrations of MSA and hence its potential contributions to particle formation in a typical coastal urban area are small compared to those of H_2SO_4 under current conditions, it will be of increasing importance as sulfur in fossil fuels decreases in response to controls.[42] In addition, MSA has been predicted to enhance particle formation from H_2SO_4 by 15−300% over the temperature range from 258 to 298 K when equivalent amounts of MSA and H_2SO_4 are present.[30] Ammonia and amines play a key role in NPF for both MSA and H_2SO_4.[18,26−29,43−52] While acid−base reactions are known to play major roles in NPF in air, it should be recognized that organics, about which less is known, may also be important.[53−61]

While the effect of temperature on NPF is important for predicting nucleation under varying atmospheric conditions both temporally (time, date, season) and spatially (longitude, latitude, altitude), our understanding of the temperature dependence of particle formation is very limited. Here, we present the first systematic study to investigate the temperature dependence of particle formation from the reaction of MSA with amines and NH_3. Overall activation energies for the formation of detectable particles (≥1.4 nm mobility diameter) from the reactions of MSA with trimethylamine (TMA), dimethylamine (DMA), methylamine (MA), and NH_3 combined with previously published quantum chemical calculations[26,29] provide some insight into the basis for the

Received: August 17, 2016
Revised: November 17, 2016
Accepted: November 18, 2016
Published: November 18, 2016

DOI: 10.1021/acs.est.6b04173
Environ. Sci. Technol. 2017, 51, 243−252

relative efficiencies of particle formation and into the atmospheric conditions where this chemistry is likely to play a role.

EXPERIMENTAL SECTION

The borosilicate glass flow reactor (briefly described in the Supporting Information) was used to study particle formation and growth over reaction times on the order of seconds at varied temperatures. Its characteristics are reported elsewhere.[27] A total flow of 17 slpm (slpm = standard liters per minute at 25 °C and 101.3 kPa) of air was used, of which 14 slpm was from ring A and ring B, 2 slpm from spokes C, and 1 slpm from spokes D (Figure S1). The source of air in these studies was dry compressed air (dew point −73 °C, $<5.2 \times 10^{13}$ cm^{-3} H_2O) from a purge air generator (model 75-62; Parker Balston) that was then passed through carbon/alumina media (Perma Pure, LLC) and a 0.1 μm filter (DIF-N70; Headline Filters) for further purification. Relative humidity was adjusted by passing part of the 14 slpm dry purified air through a bubbler filled with Nanopure water (>18.0 MΩ cm; model 7146; Thermo Scientific). Prior to introduction of the gaseous bases through spokes D to initiate particle formation and growth, a mixture of MSA flow and dry purified air was introduced through spokes C at a flow of 2 slpm for 2−3 days to passivate the walls of the inlet and the flow reactor and minimize wall losses of MSA. Particle formation was examined at 28, 26, 23.5, and 21 °C by decreasing the temperature of the circulating water within the water jacket in a stepwise fashion while keeping all other factors constant, including the system pressure and the absolute amount of water vapor. The temperature in the flow reactor was measured to be the same as that of water in the circulating jacket, consistent with characterization studies of the flow system that indicate that convection driven by temperature gradients across the cross-sectional area of the reactor is not important.[27] The change in number concentrations of MSA, base, and water vapor in molecules cm^{-3} from 21 to 28 °C is ∼2% (the mixing ratios remain constant), and concentrations reported here are those calculated for 23.5 °C. Because temperature has a significant negative effect on particle formation as discussed later, the range of precursor concentrations and temperatures that could be studied here was limited. Concentrations of gaseous precursors were adjusted to form enough particles to be detected at the highest temperature (28 °C) on our experimental time scales but not exceed 10^7 particles cm^{-3} at the lowest temperature (21 °C) to minimize particle coagulation. The relatively small change in temperature has a negligible effect on wall losses of gaseous precursors and particles as discussed in the Supporting Information (Figure S2). A portion of the sampling tube outside the flow reactor was not temperature controlled, but control experiments show that this does not produce significant artifacts (Figure S3, details shown in Supporting Information).

Dry purified air was passed over MSA liquid (99.0%, Fluka) contained in a trap at ambient temperature (∼23.5 °C) to create gas-phase MSA with the MSA concentration adjusted by changing the air flow rate. Amines/ammonia standards were generated by passing a steady flow of dry purified air through a U-shaped glass tube that held a permeation tube (VICI AG International) containing the selected base which was immersed in a water bath either at ambient temperature or at 30 °C to ensure a constant permeation rate. The following anhydrous compounds were used by the provider to prepare the permeation tubes: TMA, 99.0% Aldrich; DMA, 99% Aldrich; MA, 98% Aldrich; NH_3, 99.99% Aldrich. The concentrations of the base in the flow reactor were adjusted by introducing measured fractions of the flow from the glass permeation tube holder into the reactor.

The concentrations of MSA and the bases directly from the sources before dilution were determined with ultra performance liquid chromatography coupled with a tandem mass spectrometer (UPLC-MS/MS, Waters) and ion chromatography (IC, Metrohm), respectively.[26,28,29,62] The concentrations of MSA and the bases in the flow reactor were then calculated based on the measured concentrations from the sources and the dilution factor. Both MSA and amines/ammonia are sticky compounds, so there may be wall losses in the flow reactor inlets and the flow reactor itself even after extensive conditioning. The calculated concentrations of MSA and amines/ammonia reported here therefore represent upper limit concentrations in the flow reactor.

The possible presence of amines or ammonia in the flow reactor from diluent air or water was examined by collection of the dry/humidified air through the sampling tube onto a low-concentration cartridge.[62] The analysis confirmed that the gas phase bases, if present, were all lower than the 10 ppt detection limit. There were no particles observed from MSA-H_2O in the absence of amines , consistent with earlier studies,[22−25] or amine-H_2O in the absence of MSA even at 21 °C, further suggesting that background contamination is negligible.

Particle number concentrations were measured with a butanol-based condensation particle counter (CPC, model 3776; TSI). The CPC was coupled either to a diethylene glycol-based particle size magnifier (PSM, model A10; Airmodus; designated PSM-CPC throughout) to measure total particles or to a scanning mobility particle sizer (designated SMPS-CPC; TSI) to determine particle number size distributions. The SMPS consists of an electrostatic classifier (model 3080; TSI) and a nano-differential mobility analyzer (model 3085; TSI) to size-select particles before sending them to the CPC. Geometric mean mobility diameters determined by the SMPS are reported here as particle diameters. The d50 cutoff size of the CPC for sucrose particles was reported by the manufacturer to be ∼2.5 nm, and the PSM has a stated d50 cutoff size of ∼1.4 nm for ammonium sulfate particles. Dilution of the particle flow with zero air right before the PSM inlet is necessary when particle number concentrations surpass 10^5 cm^{-3} (approaching the upper detection limit of the CPC).

Figure S4 shows typical particle number concentrations from MSA and the amines/ammonia: TMA (Figure S4a), DMA (Figure S4b), MA (Figure S4c), and NH_3 (Figure S4d) measured either using the CPC alone or coupled to PSM under dry or humid conditions at ambient temperature (∼23.5 °C). The initial concentrations of both MSA and the selected bases were similar across experiments in order to make direct comparisons. Consistent with our previous study,[29] which could only measure particles ≥2.5 nm, the effectiveness of each base in forming particles is in the order of MA ≫ TMA ≈ DMA ≫ NH_3. The CPC alone and PSM-CPC data were within experimental error for TMA and DMA, indicating that particles had grown to diameters larger than 2.5 nm under the experimental conditions. There were some differences between the CPC only and PSM-CPC data for MA under all conditions studies, and NH_3 under low or zero added water vapor, indicating that under these reaction conditions there were particles smaller than 2.5 nm. In the temperature dependence

DOI: 10.1021/acs.est.6b04173
Environ. Sci. Technol. 2017, 51, 243−252

Table 1. Summary of Experiments, Rates, and Overall Activation Energies for Particle Formation from MSA and Amines/Ammonia

base	[MSA][a] (10^{10} cm^{-3})	[base][a] (10^{10} cm^{-3})	[H_2O] (10^{17} cm^{-3})	diameter[b] (nm)	J (cm^{-3} s^{-1}) at different temperatures[c] 28 °C	26 °C	23.5 °C	21 °C	$E_{overall}$ ($\pm1\sigma$) (kcal mol^{-1})
TMA[d]	10.4	10.4	dry	5–15	4.9(2)	1.2(3)	4.3(4)	1.9(5)	−(161 ± 23)
	10.1	10.4	dry	5–13	1.1(2)	3.4(2)	6.7(3)	5.1(4)	−(160 ± 13)
	24.9	6.4	dry	5–15	e	9.7(1)	3.9(3)	3.7(4)	−(208 ± 30)
	7.9	21.5	dry	4–12	e	1.1(2)	3.5(3)	1.5(4)	−(172 ± 41)
	7.7	8.6	2.9	7–21	4.6(2)	1.0(3)	2.6(4)	3.6(5)	−(175 ± 20)
	11.6	12.8	3.0	7–24	6.8(3)	4.4(4)	6.9(5)	5.7(6)	−(172 ± 7)
	18.0	9.6	2.8	8–32	4.7(3)	3.8(4)	3.3(5)	2.2(6)	−(153 ± 8)
	6.9	32.4	2.9	6–16	1.0(3)	4.4(3)	2.4(4)	3.8(5)	−(146 ± 12)
									average: −(168 ± 19)
DMA	12.8	12.4	dry	f	4.5(2)	2.1(3)	5.7(3)	4.7(4)	−(112 ± 11)
	9.1	12.4	dry	f	2.9(1)	1.1(2)	1.1(3)	9.4(3)	−(148 ± 5)
	5.9	6.2	dry	f	1.2(1)	1.3(2)	2.3(3)	8.3(3)	−(167 ± 21)
	4.0	4.9	2.9	4–11	2.9(2)	8.8(2)	1.5(3)	1.7(4)	−(95 ± 19)
	6.7	6.9	2.9	5–17	2.1(3)	3.4(3)	2.1(4)	1.2(5)	−(105 ± 12)
	7.7	9.9	3.0	6–17	5.6(2)	7.8(3)	1.0(5)	5.2(5)	−(172 ± 19)
	10.9	4.0	2.9	6–18	1.8(3)	2.7(3)	1.8(4)	1.7(5)	−(118 ± 17)
	2.2	31.1	3.0	f	1.1(1)	2.1(1)	3.5(2)	3.8(3)	−(153 ± 18)
									average: −(134 ± 30)
MA	5.9	1.7	dry	f	5.7(4)	1.3(5)	2.5(5)	3.2(5)	−(43 ± 9)
	4.2	6.2	dry	f	1.6(4)	2.6(4)	9.0(4)	9.4(4)	−(49 ± 12)
	4.4	3.5	dry	f	1.3(3)	4.1(3)	1.2(4)	2.8(4)	−(77 ± 7)
	1.0	1.2	3.0	f	1.3(4)	2.6(4)	7.1(4)	1.3(5)	−(60 ± 5)
	3.5	0.5	3.0	f	3.1(3)	6.8(3)	2.5(4)	9.9(4)	−(88 ± 4)
	0.7	3.0	3.0	f	6.7(4)	1.0(5)	2.5(5)	5.2(5)	−(53 ± 3)
	1.0	2.5	2.9	f	7.9(2)	1.9(3)	1.2(4)	4.3(4)	−(104 ± 7)
									average: −(68 ± 23)
NH_3	13.1	18.8	dry	f	5.0(3)	2.7(4)	1.2(5)	1.1(6)	−(132 ± 7)
	9.6	72.4	dry	f	3.9(2)	9.4(2)	4.5(3)	2.6(4)	−(107 ± 7)
	5.7	7.9	dry	4–11	2.4(2)	7.2(2)	2.9(3)	1.4(4)	−(101 ± 2)
	14.8	11.6	2.8	5–14	2.7(4)	1.1(5)	4.3(5)	1.6(6)	−(102 ± 4)
	7.7	21.7	2.9	5–13	1.6(4)	4.8(4)	1.6(5)	6.0(5)	−(90 ± 2)
	15.1	4.0	3.0	4–16	2.4(4)	1.9(5)	1.3(6)	5.8(6)	−(137 ± 12)
	2.2	50.6	2.9	3–8	6.2(3)	1.5(4)	6.0(4)	3.9(5)	−(104 ± 8)
	2.2	15.6	2.9	3–6	4.0(3)	1.0(4)	3.7(4)	2.4(5)	−(103 ± 8)
									average: −(110 ± 16)

[a]Measured at the sources and therefore represent upper limits for the concentrations given the possible losses in flow reactor inlets and the flow reactor itself. [b]Range of geometric mean diameter of particles over reaction times of 0.4–5.9 s. Typical data for particle diameter as a function of time are shown in Figures S5 and S9 in the Supporting Information. [c]Particle formation rates J calculated from number concentration−time plots as discussed in the text. Further, 4.94(2) = 4.94 × 10^2. [d]Values of J for TMA may underestimated, as discussed in the text. [e]Too few particles to be detected by SMPS (<5 × 10^3 cm^{-3}); therefore, particle formation rates cannot be derived. [f]Particle number concentrations measured with PSM-CPC rather than SMPS due to the presence of either few or small particles. The efficiency of the PSM as a function of particle size was not measured in these studies but is known to depend on both particle size[78] and composition.[79] If the number concentrations measured using PSM are underestimated by the same factor, the slope of the log J vs $1/T$ plots and the overall activation energy derived will not change.

studies discussed later, particle number concentrations were measured with either the PSM-CPC or SMPS-CPC depending on the size and number of particles formed. Particle number concentration typically shows a linear increase with time. Rates of formation of detectable particles (J) in units of cm^{-3} s^{-1} were estimated using the linear regions of the number concentration−time profiles. By doing this, particles are inherently defined as those detected by PSM-CPC or SMPS-CPC.

In previous studies from this lab,[26−29] custom gas mixtures of the individual bases in N_2 were provided by commercial gas suppliers, but significant problems were later encountered both in terms of their true concentrations and with contamination from NH_3 or other amines than the one ordered and specified on the tank by the manufacturer. The source of contaminants in the tanks according to one gas supplier was that the gas cylinders had previously been used for these contaminant species and there must have been carryover. Yu et al.[51] showed that a combination of NH_3 and DMA gave enhanced particle formation compared to what is expected for the sum of the two acting individually, and Glasoe et al.[52] reported that particle formation from H_2SO_4 and DMA or MA was enhanced by 1−3 orders of magnitude by the addition of 0.2 ppb NH_3. Thus, the presence of such contaminants can have significant effects. As a result, a changeover to the use of permeation tubes was made in the current studies, where such problems have not been encountered. The number concentrations of particles in the present study are up to several orders of magnitude lower compared to those of previous studies for TMA and DMA,[28,29]

DOI: 10.1021/acs.est.6b04173
Environ. Sci. Technol. 2017, 51, 243−252

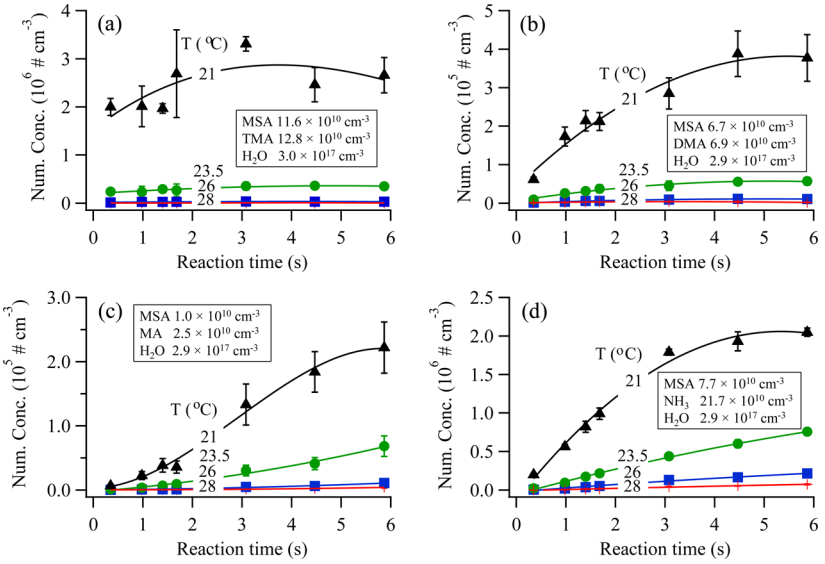

Figure 1. Typical examples of number concentrations of particles as a function of time at varied temperatures from (a) 11.6×10^{10} cm^{-3} MSA, 12.8×10^{10} cm^{-3} TMA, and 3.0×10^{17} cm^{-3} H_2O; (b) 6.7×10^{10} cm^{-3} MSA, 6.9×10^{10} cm^{-3} DMA, and 2.9×10^{17} cm^{-3} H_2O; (c) 1.0×10^{10} cm^{-3} MSA, 2.5×10^{10} cm^{-3} MA, and 2.9×10^{17} cm^{-3} H_2O; (d) 7.7×10^{10} cm^{-3} MSA, 21.7×10^{10} cm^{-3} NH_3, and 2.9×10^{17} cm^{-3} H_2O. The lines between data points are drawn as guides to the eye. Error bars represent one standard deviation from triplicate SMPS measurements and lie within the symbols in some cases.

which may be due to ammonia in the cylinder gas mixtures that was unrecognized at the time of the previous experiments. Thus, in one MSA-TMA and one MSA-DMA experiment where the amines were from permeation tubes, NH_3 was added, and large increases in particles were observed. However, as shown by the data in Figure S4, the conclusions from previous studies are robust, i.e., that water greatly enhances particle formation and the efficiency of the amines in forming particles follows the order MA > TMA ≈ DMA > NH_3.[26,28,29]

RESULTS AND DISCUSSION

The temperature dependence of the formation and growth of detectable particles was studied under a range of initial conditions shown in Table 1. Typical data for particle formation as a function of time at different temperatures are shown in Figure 1 for reactions of MSA with TMA (Figure 1a), DMA (Figure 1b), MA (Figure 1c), and NH_3 (Figure 1d) at a water vapor concentration of $2.9-3.0 \times 10^{17}$ cm^{-3}, corresponding to a relative humidity of 41−42%, respectively, if at 23.5 °C. Expanded plots for the data at temperatures from 23.5−28 °C are shown in Figure S5. Similar data under dry conditions are shown in the Supporting Information for TMA (Figure S6), DMA (Figure S7), MA (Figure S8), and NH_3 (Figure S9). SMPS-CPC data showed particle growth with time for TMA, DMA, and NH_3 (Figure S10); the ranges of diameters are summarized in Table 1 (particles from MA were too small to measure size distributions by SMPS). Once new particles are formed, there is a competition between uptake of the precursors to existing particles to grow them and formation of new clusters and particles. Note that although the d50 cutoff size of SMPS is 2.5 nm, it was only used when there were no detectable particles smaller than 2.5 nm present (Table 1).

For all of these bases, decreasing temperature significantly enhances the formation of detectable particles. Based on the Arrhenius equation ($k = A\exp(-E_{overall}/RT)$), this indicates that the effective overall activation energy for the net processes that lead from the gas phase precursors to the formation of detectable particles is negative.

Rates of formation of detectable particles (J) in units of cm^{-3} s^{-1} were estimated from plots such as those in Figure 1. Particle number concentrations from MSA and TMA level off quickly (Figure 1a), indicating that the initial rate of particle formation was too fast to be captured by the shortest sampling times. However, particles kept growing with time (Figure S10a), suggesting condensational growth of MSA-TMA particles dominated over nucleation once particles grow large enough, which is consistent with the larger diameters (Table 1). In this case, the values of J were estimated by taking the total particle number concentrations at the first measurement time of 0.4 s and dividing by 0.4 s. If particle number concentration levels off before 0.4 s, the calculation would underestimate individual values of J for the TMA reaction. However, if all of the initial rates are underestimated by the same proportion, the slope of ln J vs $1/T$ and hence overall activation energy would not be affected.

In the case of MA (Figure 1c), concentrations of gaseous precursors were kept below those which formed high particle concentrations where coagulation becomes significant. This use of low concentrations results in an apparent induction period at short reaction times before particle number concentrations linearly increase; this is at least in part due to the fact that nucleation of MSA-MA(-H_2O) is so efficient that more and smaller particles (as indicated by the difference between the PSM-CPC and CPC-only data in Figure S4) were formed at short reaction times compared to those of the other amines. The apparent induction time represents time required for MSA-MA(-H_2O) clusters to grow into detectable size particles. Thus, for MA, the linear portion of the curve after the induction time was used to obtain the particle formation rate.

Figure 2 shows plots of ln J vs $1/T$ for the amines and ammonia calculated from data in Figure 1. Overall activation energies $E_{overall}$ were calculated from the slopes of these plots and are summarized in Table 1. It is noteworthy that while

DOI: 10.1021/acs.est.6b04173
Environ. Sci. Technol. 2017, 51, 243−252

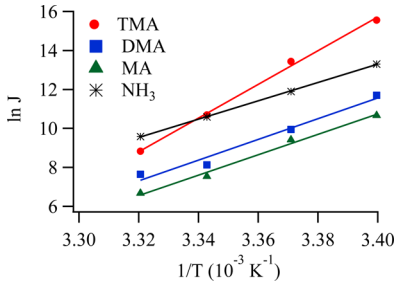

Figure 2. Plots of ln J vs the reciprocal absolute temperature $(1/T)$ with the corresponding linear fits for the reactions of MSA with amines and ammonia. Particle formation rates J were calculated from data in Figure 1, as described in the text.

different approaches were used to calculate the values of J due to the different time profiles in Figures 1a–d, overall activation energies reflect the temperature dependence of J calculated with a uniform approach within each base. This should minimize possible systematic errors. The overall activation energies do not show a significant trend with the concentrations of gaseous precursors. The average values of $E_{overall}$ are TMA, $-(168 \pm 19)$ kcal mol^{-1}; DMA, $-(134 \pm 30)$ kcal mol^{-1}; MA, $-(68 \pm 23)$ kcal mol^{-1}; and NH_3, $-(110 \pm 16)$ kcal mol^{-1} $(\pm 1\sigma)$.

For simple gas phase reaction systems, interpretation of negative activation energies is relatively straightforward. For example, consider a mechanism consisting of the following reactions:

$$A + B \underset{k_{-1}}{\overset{k_1}{\leftrightarrow}} AB \quad (1)$$

$$AB + C \xrightarrow{k_2} ABC \quad (2)$$

This is the classic case of gas phase termolecular reactions. Assuming that AB is in steady state, the overall activation energy can be shown[3] to be given by $E_{overall} \sim (E_1 + E_2 - E_{-1})$, where E_1, E_{-1}, and E_2 are the activation energies for the individual steps. If E_1 and E_2 are small so that $(E_1 + E_2) < E_{-1}$, an apparent negative activation energy results.

Consider a slightly more complicated system where ABC is also an intermediate that can decompose (reaction 3) or undergo further reaction (reaction 4):

$$ABC \xrightarrow{k_3} (AB + C) \text{ or } (AC + B) \text{ or } (A + BC) \quad (3)$$

$$ABC + D \xrightarrow{k_4} ABCD \quad (4)$$

Note that the decomposition of AB or ABC need not be back to the original reactants. This is relevant to the MSA-base-H_2O system where the reacting species are likely MSA·H_2O and base, but as discussed below, decomposition of MSA·base·H_2O may involve evaporation of water. If the species ABCD is the final "product" that does not evaporate or further react/grow in this scheme, then its rate of formation is given by

$$\frac{d[ABCD]}{dt} = k_4[ABC][D] \quad (I)$$

where the steady-state concentration of ABC is $[ABC]_{ss} = (k_2/k_{loss\_ABC}) \times [AB][C]$ and k_{loss_ABC} is the rate constant for the net loss of ABC via decomposition (reaction 3) and reaction 4 with a D molecule, i.e., $k_{loss\_ABC} = (k_3 + k_4[D])$. Assuming that ABC decomposes much faster than its reaction with D, i.e., $k_3 \gg k_4[D]$, the loss rate constant for ABC, $k_{loss\_ABC} \approx k_3$. If AB is mainly formed from reaction 1, the steady-state AB concentration is given by $[AB]_{ss} = (k_1/k_{loss\_AB})[A][B]$, where $k_{loss\_AB} \approx k_{-1}$ if the decomposition of AB is faster than its bimolecular reaction 2. Then, the rate of formation of ABCD becomes

$$\frac{d[ABCD]}{dt} = k_4[ABC][D] \approx \frac{k_1k_2k_4}{k_3k_{-1}}[A][B][C][D] \quad (II)$$

Assuming the Arrhenius expression applies to the individual steps over the limited temperature range used here, the effective overall rate constant is given by

$$k_{overall} = \frac{k_1k_2k_4}{k_3k_{-1}} = \frac{A_1A_2A_4}{A_3A_{-1}}\exp\left[-\frac{(E_1 + E_2 + E_4) - (E_3 + E_{-1})}{RT}\right] \quad (III)$$

The overall activation energy is then the difference between the sum of those for the forward reactions and the sum of those for the decomposition reactions of the intermediates.

The kinetically simplest hypothetical case is the one in which the bimolecular reactions 1, 2, and 4 have a zero, or very small, activation energies. In this case, the overall activation energy is approximated by $-(E_3 + E_{-1})$ where these terms reflect the energy differences between the clusters and the species to which they decompose (Figure 3). If similar considerations

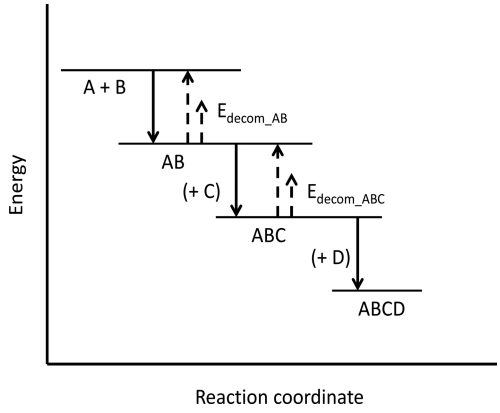

Figure 3. Schematic of simplified reaction scheme for a hypothetical reaction scheme involving the formation of intermediate clusters AB and ABC that can decompose or continue to react to form the final product ABCD. The enthalpy of the forward reactions ΔH is related to the change in energy ΔE via $\Delta H = \Delta E + \Delta nRT$.

apply for a reaction mechanism with many more clusters and steps, the overall negative activation energy is a measure of the sum of the energies required for decomposition of each cluster.

While eq III shows conceptually how the overall activation energy for a complex reaction scheme is qualitatively related to those for the individual reactions, the quantitative relationship is clearly sensitive to the mechanism and relative importance of various steps. As a result, extrapolation of this simplified approach to the MSA-amine(-H_2O) system is not straightforward. First, decomposition of clusters can occur by many different pathways, including evaporation of monomers or ejection of smaller clusters (growth can also occur via uptake of clusters).[63−66] Second, the composition of clusters that affect

DOI: 10.1021/acs.est.6b04173
Environ. Sci. Technol. 2017, 51, 243−252

particle formation may not be constant over the range of temperatures studied, even though this range is relatively small. Third, the decomposition of clusters is assumed to be temperature dependent, and the forward reactions are assumed to proceed with zero or small activation energy; the connection between overall activation energy and those for the individual steps becomes less direct if the activation energies for the forward steps are not small. Fourth, the energetics for loss of single molecules can change as the clusters become larger. Finally, given the dynamic nature of the system, with precursor gases both forming new particles and adding to existing ones to grow them as well as the uncertainties in deriving particle formation rates from data which are not always linear throughout the time range studied, steady-state assumptions may not be rigorously applicable. However, the concept of a negative temperature dependence for particle formation being due to decreasing cluster stability with increasing temperature is consistent with the generic reaction scheme above and with interpretation of the temperature dependence of particle formation in sulfuric acid-amine systems.[67]

In the case of particle formation from sulfuric acid, a stepwise mechanism[53] similar to the simple reaction scheme above is believed to occur, and the mechanism for particle formation from MSA is expected to have qualitative similarities.[26,28] In the case of sulfuric acid clusters with ammonia or DMA, evaporation of one or more of the components can occur depending on the conditions.[68] For example, quantum chemical calculations for such clusters show that if the number of base molecules is equal to or greater than the number of acid molecules, evaporation of the base dominates, while with excess acid in the cluster, the acid can evaporate.[63,69] If water is present, it can also evaporate.[68]

MSA is known to form hydrates[22,24,25] so that when water is present, the MSA hydrate in equilibrium with MSA is likely the initial reacting species (equivalent to A in Figure 3). The water vapor concentration is essentially constant in the flow system so that the hydrate concentration is determined by that of MSA. Shown below are a few potential initial steps in the mechanism, which includes both addition of monomers (equivalent to C and D in Figure 3) to clusters to grow them, and the decomposition of the clusters (shown by the vertical dotted lines in Figure 3):

$$\mathrm{MSA} + \mathrm{H_2O} \leftrightarrow \mathrm{MSA{\cdot}H_2O} \quad (5)$$

$$\mathrm{MSA{\cdot}H_2O} + \mathrm{base} \leftrightarrow \mathrm{MSA{\cdot}base{\cdot}H_2O} \quad (6)$$

$$\mathrm{MSA{\cdot}base{\cdot}H_2O} + \mathrm{MSA} \leftrightarrow (\mathrm{MSA})_2{\cdot}\mathrm{base{\cdot}H_2O} \quad (7)$$

$$\mathrm{MSA{\cdot}base{\cdot}H_2O} + \mathrm{base} \leftrightarrow \mathrm{MSA{\cdot}(base)_2{\cdot}H_2O} \quad (8)$$

$$\mathrm{MSA{\cdot}base{\cdot}H_2O} + \mathrm{H_2O} \leftrightarrow \mathrm{MSA{\cdot}base{\cdot}(H_2O)_2} \quad (9)$$

For the MSA-amine(-H_2O) system, the binding energies are known only for the first few steps. Taking the MSA-TMA reaction as an example, the enthalpies for the evaporation of MSA, TMA, and H_2O from a MSA·TMA·H_2O cluster are ~27, ~23, and ~13 respectively.[26,29] Enthalpy and energy changes differ only by a small amount because they are related by $\Delta H = \Delta E + \Delta nRT$, where the last term is 0.6 kcal mol^{-1} at 298 K for $\Delta n = 1$. The enthalpies of evaporation of MSA, TMA, and H_2O from a $(MSA)_2$·TMA·H_2O cluster are ~25, ~32, and ~14, respectively.[26,29] Thus, loss of water seems likely for both clusters. For the 1:1:1 cluster, loss of MSA is least favored, while for the 2:1:1 cluster, loss of TMA is least likely on energetic grounds.

The overall activation energy will be some combination of the energies for evaporation of acid, base, water, or clusters in each elemental step and the total number of reversible steps that lead to particle formation. The fact that the overall activation energies are similar regardless of the addition of water (Table 1) has a number of possible explanations. For example, evaporation of base or acid rather than water could dominate in both cases so that water does not have a significant effect. Alternatively, while the individual contributions of the average energy per decomposition step and the total number of steps involved in particle formation may be different with and without water, their combination, which determines the overall activation energy, may be similar. This could occur if there are different evaporation routes, e.g., involving ejection of clusters vs monomers.

The observation that formation of MSA-MA particles has an $E_{overall}$ [−(68 ± 23) kcal mol^{-1}] much smaller than that of MSA-TMA particles [−(168 ± 19) kcal mol^{-1}] could be due to different energies for the individual decomposition steps for the different amines and/or to a smaller number of steps to form detectable particles in the case of MA. The limited thermodynamic data on the smallest clusters in these systems[26,29] do not suggest large thermodynamic differences for clusters of the same composition for the different amines. Thus, the difference in $E_{overall}$ is more likely to be due to fewer reversible elemental steps to form detectable MSA-MA particles. This is consistent with MA forming particles more efficiently compared to DMA and TMA.

The relatively few studies of the temperature dependence of detectable particles from reactions of H_2SO_4 with ammonia or amines also give negative activation energies in agreement with the increased decomposition of clusters with increasing temperature.[67] However, the absolute values of $E_{overall}$ are smaller for the sulfuric acid reactions. For example, data on neutral particle formation in the H_2SO_4-NH_3 reaction at 278, 288, and 292 K in Kirkby et al. (cf. Figure 1)[47] suggests $E_{overall}$ for particle formation of −(35−40) kcal mol^{-1}, which is considerably smaller than the −110 kcal mol^{-1} for the MSA-NH_3-H_2O reaction reported here. For the H_2SO_4-DMA reaction, Almeida et al.[18] report a relatively small calculated temperature dependence for the combination of neutral and galactic cosmic ray-induced reactions with the rate constant predicted to fall by about a factor of 2 from 21 to 28 °C rather than by several orders of magnitude as for MSA reported here. One reason may be that MSA·base·H_2O clusters are less stable, and evaporation of the monomer or cluster is faster. For example, the ΔH calculated[29] for formation of the MSA·DMA·H_2O cluster from the gas precursors is −36 kcal mol^{-1} compared to −43 kcal mol^{-1} for the analogous H_2SO_4 1 acid·1 base·1 water cluster.[70] For the 2 acid·1 base·1 water cluster for MSA and DMA,[26] ΔH is ~ −61 kcal mol^{-1} compared to −74 kcal mol^{-1} for the H_2SO_4 cluster.[70]

Although further laboratory and theoretical studies are needed to develop more detailed mechanistic insights, the anticorrelation between particle formation and temperature suggests that the rate of particle formation from MSA and amines/ammonia will be temporally and spatially regulated in the atmosphere with particle formation being more efficient in winter and at higher altitudes, all other factors being equal. However, the concentrations of both MSA and amines/NH_3 are likely to decrease with altitude because their sources are at

DOI: 10.1021/acs.est.6b04173
Environ. Sci. Technol. 2017, 51, 243−252

the Earth's surface, and the source strengths are also dependent on location and season. For example, the major source of MSA is the oxidation of organosulfur compounds generated by oceanic biological processes with fluxes to the atmosphere enhanced in the spring and summer.[71] The major sources of amines are also at the surface.[72] Field measurements have shown particulate methanesulfonate decreases with altitude,[73,74] as do ammonia and model-predicted amine concentrations.[75−77] This relationship between reduced concentrations and temperature will result in counterbalancing of the two effects in particle formation. However, the significantly increased efficiencies at lower temperatures does mean that many more particles will be formed than otherwise expected based solely on precursor concentrations and ambient temperature experiments. These results illustrate the importance of taking into account temperature along with other factors such as the nature and concentrations of nucleation precursors, relative humidity, and the availability of pre-existing particles in modeling studies to better predict new particle formation and its impacts on health, visibility, and climate.

■ ASSOCIATED CONTENT

Supporting Information

The Supporting Information is available free of charge on the ACS Publications website at DOI: 10.1021/acs.est.6b04173.

Schematic and description of the flow reactor (Figure S1), effect of temperature on wall losses of gaseous precursors and particles (Figure S2), effect of the sampling tube temperature (Figure S3), particle number concentrations as a function of time measured by PSM-CPC and CPC only (Figure S4), expanded view of particle number concentrations as a function of time at the higher temperatures for the data shown in Figures 1a−d (Figure S5), particle number concentrations as a function of time at varied temperatures under dry conditions (Figures S6−S9), particle diameters as a function of time under humid conditions (Figure S10), and estimated diffusion coefficients for gas phase precursors at varied temperatures (Table S1) (PDF)

■ AUTHOR INFORMATION

Corresponding Author

*Phone: (949) 824-7670; fax: (949) 824-2420; e-mail: bjfinlay@uci.edu.

ORCID

Barbara J. Finlayson-Pitts: 0000-0003-4650-168X

Notes

The authors declare no competing financial interest.

■ ACKNOWLEDGMENTS

The authors are grateful to the National Science Foundation (Grants 0909227 and 1443140) for funding. We are very grateful to Dr. Mychel E. Varner and Dr. R. Benny Gerber for helpful discussions, Kristine Arquero and Dr. Véronique Perraud for technical assistance, and Metrohm USA for their support and help in ion chromatography analysis.

■ REFERENCES

(1) Zhang, R.; Khalizov, A.; Wang, L.; Hu, M.; Xu, W. Nucleation and growth of nanoparticles in the atmosphere. *Chem. Rev.* **2012**, *112* (3), 1957−2011.

(2) Kulmala, M.; Vehkamäki, H.; Petäjä, T.; Dal Maso, M.; Lauri, A.; Kerminen, V.-M.; Birmili, W.; McMurry, P. H. Formation and growth rates of ultrafine atmospheric particles: a review of observations. *J. Aerosol Sci.* **2004**, *35* (2), 143−176.

(3) Finlayson-Pitts, B. J.; Pitts, Jr., J. N. *Chemistry of the Upper and Lower Atmosphere: Theory, Experiments, and Applications*; Academic Press: San Diego, CA, 2000.

(4) Seinfeld, J. H.; Pandis, S. N. *Atmospheric Chemistry and Physics: From Air Pollution to Climate Change*; John Wiley & Sons: New York, 2006.

(5) Farmer, D. K.; Cappa, C. C.; Kreidenweis, S. M. Atmospheric processes and their controlling influence on cloud condensation nuclei activity. *Chem. Rev.* **2015**, *115*, 4199−4217.

(6) Kerminen, V.-M.; Lihavainen, H.; Komppula, M.; Viisanen, Y.; Kulmala, M. Direct observational evidence linking atmospheric aerosol formation and cloud droplet activation. *Geophys. Res. Lett.* **2005**, *32* (14), L14803.

(7) Spracklen, D. V.; Carslaw, K. S.; Kulmala, M.; Kerminen, V.-M.; Sihto, S.-L.; Riipinen, I.; Merikanto, J.; Mann, G. W.; Chipperfield, M. P.; Wiedensohler, A.; Birmili, W.; Lihavainen, H. Contribution of particle formation to global cloud condensation nuclei concentrations. *Geophys. Res. Lett.* **2008**, *35* (6), L06808.

(8) Kuang, C.; McMurry, P. H.; McCormick, A. V. Determination of cloud condensation nuclei production from measured new particle formation events. *Geophys. Res. Lett.* **2009**, *36* (9), L09822.

(9) Merikanto, J.; Spracklen, D. V.; Mann, G. W.; Pickering, S. J.; Carslaw, K. S. Impact of nucleation on global CCN. *Atmos. Chem. Phys.* **2009**, *9* (21), 8601−8616.

(10) Pöschl, U. Atmospheric aerosols: composition, transformation, climate and health effects. *Angew. Chem., Int. Ed.* **2005**, *44*, 7520−7540.

(11) Heal, M. R.; Kumar, P.; Harrison, R. M. Particles, air quality, policy and health. *Chem. Soc. Rev.* **2012**, *41*, 6606−6630.

(12) Kuang, C.; McMurry, P. H.; McCormick, A. V.; Eisele, F. L. Dependence of nucleation rates on sulfuric acid vapor concentration in diverse atmospheric locations. *J. Geophys. Res.* **2008**, *113*, D10209.

(13) Sipilä, M.; Berndt, T.; Petäjä, T.; Brus, D.; Vanhanen, J.; Stratmann, F.; Patokoski, J.; Mauldin, R. L.; Hyvarinen, A. P.; Lihavainen, H.; Kulmala, M. The role of sulfuric acid in atmospheric nucleation. *Science* **2010**, *327* (5970), 1243−1246.

(14) Weber, R. J.; Chen, G.; Davis, D. D.; Mauldin, R. L., III; Tanner, D. J.; Eisele, F. L.; Clarke, A. D.; Thornton, D. C.; Bandy, A. R. Measurements of enhanced H_2SO_4 and 3−4 nm particles near a frontal cloud during the First Aerosol Characterization Experiment (ACE 1). *J. Geophys. Res.* **2001**, *106* (D20), 24107−24117.

(15) Weber, R. J.; Marti, J. J.; McMurry, P. H.; Eisele, F. L.; Tanner, D. J.; Jefferson, A. Measured atmospheric new particle formation rates: Implications for nulceation mechanisms. *Chem. Eng. Commun.* **1996**, *151* (1), 53−64.

(16) Weber, R. J.; Marti, J. J.; McMurry, P. H.; Eisele, F. L.; Tanner, D. J.; Jefferson, A. Measurements of new particle formation and ultrafine particle growth rates at a clean continental site. *J. Geophys. Res.* **1997**, *102* (D4), 4375−4385.

(17) Kulmala, M.; Lehtinen, K. E. J.; Laaksonen, A. Cluster activation theory as an explanation of the linear dependence between formation rate of 3 nm particles and sulphuric acid concentration. *Atmos. Chem. Phys.* **2006**, *6* (3), 787−793.

(18) Almeida, J.; Schobesberger, S.; Kürten, A.; Ortega, I. K.; Kupiainen-Määttä, O.; Praplan, A. P.; Adamov, A.; Amorim, A.; Bianchi, F.; Breitenlechner, M.; David, A.; Dommen, J.; Donahue, N. M.; Downard, A.; Dunne, E.; Duplissy, J.; Ehrhart, S.; Flagan, R. C.; Franchin, A.; Guida, R.; Hakala, J.; Hansel, A.; Heinritzi, M.; Henschel, H.; Jokinen, T.; Junninen, H.; Kajos, M.; Kangasluoma, J.; Keskinen, H.; Kupc, A.; Kurtén, T.; Kvashin, A. N.; Laaksonen, A.; Lehtipalo, K.; Leiminger, M.; Leppä, J.; Loukonen, V.; Makhmutov, V.; Mathot, S.; McGrath, M. J.; Nieminen, T.; Olenius, T.; Onnela, A.; Petäjä, T.; Riccobono, F.; Riipinen, I.; Rissanen, M.; Rondo, L.; Ruuskanen, T.; Santos, F. D.; Sarnela, N.; Schallhart, S.; Schnitzhofer, R.; Seinfeld, J. H.; Simon, M.; Sipilä, M.; Stozhkov, Y.; Stratmann, F.; Tomé, A.; Tröstl, J.; Tsagkogeorgas, G.; Vaattovaara, P.; Viisanen, Y.; Virtanen,

DOI: 10.1021/acs.est.6b04173
Environ. Sci. Technol. 2017, 51, 243−252

A.; Vrtala, A.; Wagner, P. E.; Weingartner, E.; Wex, H.; Williamson, C.; Wimmer, D.; Ye, P.; Yli-Juuti, T.; Carslaw, K. S.; Kulmala, M.; Curtius, J.; Baltensperger, U.; Worsnop, D. R.; Vehkamäki, H.; Kirkby, J. Molecular understanding of sulphuric acid-amine particle nucleation in the atmosphere. *Nature* **2013**, *502* (7471), 359−363.
(19) Bzdek, B. R.; Horan, A. J.; Pennington, M. R.; DePalma, J. W.; Zhao, J.; Jen, C. N.; Hanson, D. R.; Smith, J. N.; McMurry, P. H.; Johnston, M. V. Quantitative and time-resolved nanoparticle composition measurements during new particle formation. *Faraday Discuss.* **2013**, *165*, 25−43.
(20) Stolzenburg, M. R.; McMurry, P. H.; Sakurai, H.; Smith, J. N.; Mauldin, R. L., III; Eisele, F. L.; Clement, C. F. Growth rates of freshly nucleated particles in Atlanta. *J. Geophys. Res.* **2005**, *110*, D22S05.
(21) Chen, M.; Titcombe, M.; Jiang, J. K.; Jen, C.; Kuang, C. A.; Fischer, M. L.; Eisele, F. L.; Siepmann, J. I.; Hanson, D. R.; Zhao, J.; McMurry, P. H. Acid-base chemical reaction model for nucleation rates in the polluted atmospheric boundary layer. *Proc. Natl. Acad. Sci. U. S. A.* **2012**, *109* (46), 18713−18718.
(22) Wyslouzil, B. E.; Seinfeld, J. H.; Flagan, R. C.; Okuyama, K. Binary nucleation in acid-water systems. I. methanesulfonic acid-water. *J. Chem. Phys.* **1991**, *94* (10), 6827−6841.
(23) Wyslouzil, B. E.; Seinfeld, J. H.; Flagan, R. C.; Okuyama, K. Binary nucleation in acid-water systems. II. sulfuric acid-water and a comparison with methanesulfonic acid-water. *J. Chem. Phys.* **1991**, *94* (10), 6842−6850.
(24) Kreidenweis, S. M.; Flagan, R. C.; Seinfeld, J. H.; Okuyama, K. Binary nucleation of methanesulfonic acid and water. *J. Aerosol Sci.* **1989**, *20* (5), 585−607.
(25) Kreidenweis, S. M.; Seinfeld, J. H. Nucleation of sulfuric acid-water and methanesulfonic acid-water solution particles: Implications for the atmospheric chemistry of organosulfur species. *Atmos. Environ.* **1988**, *22* (2), 283−296.
(26) Dawson, M. L.; Varner, M. E.; Perraud, V.; Ezell, M. J.; Gerber, R. B.; Finlayson-Pitts, B. J. Simplified mechanism for new particle formation from methanesulfonic acid, amines, and water via experiments and Ab initio calculations. *Proc. Natl. Acad. Sci. U. S. A.* **2012**, *109* (46), 18719−18724.
(27) Ezell, M. J.; Chen, H.; Arquero, K. D.; Finlayson-Pitts, B. J. Aerosol fast flow reactor for laboratory studies of new particle formation. *J. Aerosol Sci.* **2014**, *78* (0), 30−40.
(28) Chen, H.; Ezell, M. J.; Arquero, K. D.; Varner, M. E.; Dawson, M. L.; Gerber, R. B.; Finlayson-Pitts, B. J. New particle formation and growth from methanesulfonic acid, trimethylamine and water. *Phys. Chem. Chem. Phys.* **2015**, *17*, 13699−13709.
(29) Chen, H.; Varner, M. E.; Gerber, R. B.; Finlayson-Pitts, B. J. Reactions of methanesulfonic acid with amines and ammonia as a source of new particles in air. *J. Phys. Chem. B* **2016**, *120* (8), 1526−1536.
(30) Bork, N.; Elm, J.; Olenius, T.; Vehkamäki, H. Methane sulfonic acid-enhanced formation of molecular clusters of sulfuric acid and dimethyl amine. *Atmos. Chem. Phys.* **2014**, *14* (22), 12023−12030.
(31) Bates, T. S.; Lamb, B. K.; Guenther, A.; Dignon, J.; Stoiber, R. E. Sulfur emissions to the atmosphere from natural sourees. *J. Atmos. Chem.* **1992**, *14* (1−4), 315−337.
(32) VanderGheynst, J. S.; Cogan, D. J.; DeFelice, P. J.; Gossett, J. M.; Walker, L. P. Effect of process management on the emission of organosulfur compounds and gaseous antecedents from composting processes. *Environ. Sci. Technol.* **1998**, *32* (23), 3713−3718.
(33) Rosenfeld, P. E.; Henry, C. L.; Dills, R. L.; Harrison, R. B. Comparison of odor emissions from three different biosolids applied to forest soil. *Water, Air, Soil Pollut.* **2001**, *127* (1−4), 173−191.
(34) Meinardi, S.; Simpson, I. J.; Blake, N. J.; Blake, D. R.; Rowland, F. S. Dimethyl disulfide (DMDS) and dimethyl sulfide (DMS) emissions from biomass burning in Australia. *Geophys. Res. Lett.* **2003**, *30* (9), 1454.
(35) Barnes, I.; Hjorth, J.; Mihalopoulos, N. Dimethyl sulfide and dimethyl sulfoxide and their oxidation in the atmosphere. *Chem. Rev.* **2006**, *106* (3), 940−975.
(36) Berresheim, H.; Elste, T.; Tremmel, H. G.; Allen, A. G.; Hansson, H. C.; Rosman, K.; Dal Maso, M.; Mäkelä, J. M.; Kulmala, M.; O'Dowd, C. D. Gas-aerosol relationships of H_2SO_4, MSA, and OH: Observations in the coastal marine boundary layer at Mace Head, Ireland. *J. Geophys. Res.* **2002**, *107* (D19), 8100.
(37) Berresheim, H.; Eisele, F. L.; Tanner, D. J.; McInnes, L. M.; Ramsey-Bell, D. C.; Covert, D. S. Atmospheric sulfur chemistry and cloud condensation nuclei (CCN) concentrations over the northeastern Pacific Coast. *J. Geophys. Res.* **1993**, *98* (D7), 12701−12711.
(38) Mauldin, R. L.; Cantrell, C. A.; Zondlo, M. A.; Kosciuch, E.; Ridley, B. A.; Weber, R.; Eisele, F. E. C. Measurements of OH, H_2SO_4, and MSA during Tropospheric Ozone Production About the Spring Equinox (TOPSE). *J. Geophys. Res.* **2003**, *108* (D4), 8366.
(39) Mauldin, R. L.; Tanner, D. J.; Heath, J. A.; Huebert, B. J.; Eisele, F. L. Observations of H_2SO_4 and MSA during PEM-Tropics-A. *J. Geophys. Res.* **1999**, *104* (D5), 5801−5816.
(40) Eisele, F. L.; Tanner, D. J. Measurement of the gas phase concentration of H_2SO_4 and methane sulfonic acid and estimates of H_2SO_4 production and loss in the atmosphere. *J. Geophys. Res.* **1993**, *98* (D5), 9001−9010.
(41) Perraud, V.; Horne, J. R.; Martinez, A.; Kalinowski, J.; Meinardi, S.; Dawson, M. L.; Wingen, L. M.; Dabdub, D.; Blake, D. R.; Gerber, R. B.; Finlayson-Pitts, B. J. The future of airborne particles in the absence of fossil fuel sulfur dioxide emissions. *Proc. Natl. Acad. Sci. U. S. A.* **2015**, *112*, 13514−13519.
(42) Stern, D. I. Global sulfur emissions from 1850 to 2000. *Chemosphere* **2005**, *58*, 163−175.
(43) Ball, S. M.; Hanson, D. R.; Eisele, F. L.; McMurry, P. H. Laboratory studies of particle nucleation: Initial results for H_2SO_4, H_2O, and NH_3 vapors. *J. Geophys. Res.* **1999**, *104* (D19), 23709−23718.
(44) Korhonen, P.; Kulmala, M.; Laaksonen, A.; Viisanen, Y.; McGraw, R.; Seinfeld, J. H. Ternary nucleation of H_2SO_4, NH_3, and H_2O in the atmosphere. *J. Geophys. Res.* **1999**, *104* (D21), 26349−26353.
(45) Benson, D. R.; Erupe, M. E.; Lee, S.-H. Laboratory-measured H_2SO_4-H_2O-NH_3 ternary homogeneous nucleation rates: Initial observations. *Geophys. Res. Lett.* **2009**, *36* (15), L15818.
(46) Berndt, T.; Stratmann, F.; Sipilä, M.; Vanhanen, J.; Petäjä, T.; Mikkilä, J.; Grüner, A.; Spindler, G.; Lee Mauldin, R., III; Curtius, J.; Kulmala, M.; Heintzenberg, J. Laboratory study on new particle formation from the reaction OH + SO_2: Influence of experimental conditions, H_2O vapour, NH_3 and the amine tert-butylamine on the overall process. *Atmos. Chem. Phys.* **2010**, *10* (15), 7101−7116.
(47) Kirkby, J.; Curtius, J.; Almeida, J.; Dunne, E.; Duplissy, J.; Ehrhart, S.; Franchin, A.; Gagné, S.; Ickes, L.; Kürten, A.; Kupc, A.; Metzger, A.; Riccobono, F.; Rondo, L.; Schobesberger, S.; Tsagkogeorgas, G.; Wimmer, D.; Amorim, A.; Bianchi, F.; Breitenlechner, M.; David, A.; Dommen, J.; Downard, A.; Ehn, M.; Flagan, R. C.; Haider, S.; Hansel, A.; Hauser, D.; Jud, W.; Junninen, H.; Kreissl, F.; Kvashin, A.; Laaksonen, A.; Lehtipalo, K.; Lima, J.; Lovejoy, E. R.; Makhmutov, V.; Mathot, S.; Mikkilä, J.; Minginette, P.; Mogo, S.; Nieminen, T.; Onnela, A.; Pereira, P.; Petäjä, T.; Schnitzhofer, R.; Seinfeld, J. H.; Sipilä, M.; Stozhkov, Y.; Stratmann, F.; Tomé, A.; Vanhanen, J.; Viisanen, Y.; Vrtala, A.; Wagner, P. E.; Walther, H.; Weingartner, E.; Wex, H.; Winkler, P. M.; Carslaw, K. S.; Worsnop, D. R.; Baltensperger, U.; Kulmala, M. Role of sulphuric acid, ammonia and galactic cosmic rays in atmospheric aerosol nucleation. *Nature* **2011**, *476* (7361), 429−433.
(48) Zollner, J. H.; Glasoe, W. A.; Panta, B.; Carlson, K. K.; McMurry, P. H.; Hanson, D. R. Sulfuric acid nucleation: Power dependencies, variation with relative humidity, and effect of bases. *Atmos. Chem. Phys.* **2012**, *12* (10), 4399−4411.
(49) Kurtén, T.; Loukonen, V.; Vehkamäki, H.; Kulmala, M. Amines are likely to enhance neutral and ion-induced sulfuric acid-water nucleation in the atmosphere more effectively than ammonia. *Atmos. Chem. Phys.* **2008**, *8* (14), 4095−4103.

DOI: 10.1021/acs.est.6b04173
Environ. Sci. Technol. 2017, 51, 243−252

(50) Erupe, M. E.; Viggiano, A. A.; Lee, S.-H. The effect of trimethylamine on atmospheric nucleation involving H_2SO_4. *Atmos. Chem. Phys.* **2011**, *11* (10), 4767−4775.
(51) Yu, H.; McGraw, R.; Lee, S.-H. Effects of amines on formation of sub-3 nm particles and their subsequent growth. *Geophys. Res. Lett.* **2012**, *39* (2), L02807.
(52) Glasoe, W. A.; Volz, K.; Panta, B.; Freshour, N.; Bachman, R.; Hanson, D. R.; McMurry, P. H.; Jen, C. Sulfuric acid nucleation: An experimental study of the effect of seven bases. *J. Geophys. Res.* **2015**, *120* (5), 1933−1950.
(53) Bianchi, F.; Praplan, A. P.; Sarnela, N.; Dommen, J.; Kurten, A.; Ortega, I. K.; Schobesberger, S.; Junninen, H.; Simon, M.; Trostl, J.; Jokinen, T.; Sipila, M.; Adamov, A.; Amorim, A.; Almeida, J.; Breitenlechner, M.; Duplissy, J.; Ehrhart, S.; Flagan, R. C.; Franchin, A.; Hakala, J.; Hansel, A.; Heinritzi, M.; Kangasluoma, J.; Keskinen, H.; Kim, J.; Kirkby, J.; Laaksonen, A.; Lawler, M. J.; Lehtipalo, K.; Leiminger, M.; Makhmutov, V.; Mathot, S.; Onnela, A.; Petaja, T.; Riccobono, F.; Rissanen, M. P.; Rondo, L.; Tome, A.; Virtanen, A.; Viisanen, Y.; Williamson, C.; Wimmer, D.; Winkler, P. M.; Ye, P. L.; Curtius, J.; Kulmala, M.; Worsnop, D. R.; Donahue, N. M.; Baltensperger, U. Insight into acid-base nucleation experiments by comparison of the chemical composition of positive, negative, and neutral clusters. *Environ. Sci. Technol.* **2014**, *48* (23), 13675−13684.
(54) Donahue, N. M.; Ortega, I. K.; Chuang, W.; Riipinen, I.; Riccobono, F.; Schobesberger, S.; Dommen, J.; Baltensperger, U.; Kulmala, M.; Worsnop, D. R.; Vehkamäki, H. How do organic vapors contribute to new-particle formation? *Faraday Discuss.* **2013**, *165*, 91−104.
(55) Ehn, M.; Thornton, J. A.; Kleist, E.; Sipilä, M.; Junninen, H.; Pullinen, I.; Springer, M.; Rubach, F.; Tillmann, R.; Lee, B.; Lopez-Hilfiker, F.; Andres, S.; Acir, I. H.; Rissanen, M.; Jokinen, T.; Schobesberger, S.; Kangasluoma, J.; Kontkanen, J.; Nieminen, T.; Kurtén, T.; Nielsen, L. B.; Jorgensen, S.; Kjaergaard, H. G.; Canagaratna, M.; Dal Maso, M.; Berndt, T.; Petäjä, T.; Wahner, A.; Kerminen, V.-M.; Kulmala, M.; Worsnop, D. R.; Wildt, J.; Mentel, T. F. A large source of low-volatility secondary organic aerosol. *Nature* **2014**, *506* (7489), 476−479.
(56) Jokinen, T.; Berndt, T.; Makkonen, R.; Kerminen, V.-M.; Junninen, H.; Paasonen, P.; Stratmann, F.; Herrmann, H.; Guenther, A. B.; Worsnop, D. R.; Kulmala, M.; Ehn, M.; Sipilä, M. Production of extremely low volatile organic compounds from biogenic emissions: Measured yields and atmospheric implications. *Proc. Natl. Acad. Sci. U. S. A.* **2015**, *112* (23), 7123−7128.
(57) Riccobono, F.; Schobesberger, S.; Scott, C. E.; Dommen, J.; Ortega, I. K.; Rondo, L.; Almeida, J.; Amorim, A.; Bianchi, F.; Breitenlechner, M.; David, A.; Downard, A.; Dunne, E. M.; Duplissy, J.; Ehrhart, S.; Flagan, R. C.; Franchin, A.; Hansel, A.; Junninen, H.; Kajos, M.; Keskinen, H.; Kupc, A.; Kürten, A.; Kvashin, A. N.; Laaksonen, A.; Lehtipalo, K.; Makhmutov, V.; Mathot, S.; Nieminen, T.; Onnela, A.; Petäjä, T.; Praplan, A. P.; Santos, F. D.; Schallhart, S.; Seinfeld, J. H.; Sipilä, M.; Spracklen, D. V.; Stozhkov, Y.; Stratmann, F.; Tomé, A.; Tsagkogeorgas, G.; Vaattovaara, P.; Viisanen, Y.; Vrtala, A.; Wagner, P. E.; Weingartner, E.; Wex, H.; Wimmer, D.; Carslaw, K. S.; Curtius, J.; Donahue, N. M.; Kirkby, J.; Kulmala, M.; Worsnop, D. R.; Baltensperger, U. Oxidation products of biogenic emissions contribute to nucleation of atmospheric particles. *Science* **2014**, *344* (6185), 717−721.
(58) Schobesberger, S.; Junninen, H.; Bianchi, F.; Lönn, G.; Ehn, M.; Lehtipalo, K.; Dommen, J.; Ehrhart, S.; Ortega, I. K.; Franchin, A.; Nieminen, T.; Riccobono, F.; Hutterli, M.; Duplissy, J.; Almeida, J.; Amorim, A.; Breitenlechner, M.; Downard, A. J.; Dunne, E. M.; Flagan, R. C.; Kajos, M.; Keskinen, H.; Kirkby, J.; Kupc, A.; Kürten, A.; Kurtén, T.; Laaksonen, A.; Onnela, A.; Praplan, A. P.; Rondo, L.; Santos, F. D.; Schallhart, S.; Schnitzhofer, R.; Sipilä, M.; Tomé, A.; Tsagkogeorgas, G.; Vehkamäki, H.; Wimmer, D.; Baltensperger, U.; Carslaw, K. S.; Curtius, J.; Hansel, A.; Petäjä, T.; Kulmala, M.; Donahue, N. M.; Worsnop, D. R. Molecular understanding of atmospheric particle formation from sulfuric acid and large oxidized organic molecules. *Proc. Natl. Acad. Sci. U. S. A.* **2013**, *110* (43), 17223−17228.
(59) Zhang, R.; Suh, I.; Zhao, J.; Zhang, D.; Fortner, E. C.; Tie, X.; Molina, L. T.; Molina, M. J. Atmospheric new particle formation enhanced by organic acids. *Science* **2004**, *304* (5676), 1487−1490.
(60) Bianchi, F.; Trostl, J.; Junninen, H.; Frege, C.; Henne, S.; Hoyle, C. R.; Molteni, U.; Herrmann, E.; Adamov, A.; Bukowiecki, N.; Chen, X.; Duplissy, J.; Gysel, M.; Hutterli, M.; Kangasluoma, J.; Kontkanen, J.; Kurten, A.; Manninen, H. E.; Munch, S.; Perakyla, O.; Petaja, T.; Rondo, L.; Williamson, C.; Weingartner, E.; Curtius, J.; Worsnop, D. R.; Kulmala, M.; Dommen, J.; Baltensperger, U. New particle formation in the free troposphere: A question of chemistry and timing. *Science* **2016**, *352* (6289), 1109−1112.
(61) Trostl, J.; Chuang, W. K.; Gordon, H.; Heinritzi, M.; Yan, C.; Molteni, U.; Ahlm, L.; Frege, C.; Bianchi, F.; Wagner, R.; Simon, M.; Lehtipalo, K.; Williamson, C.; Craven, J. S.; Duplissy, J.; Adamov, A.; Almeida, J.; Bernhammer, A. K.; Breitenlechner, M.; Brilke, S.; Dias, A.; Ehrhart, S.; Flagan, R. C.; Franchin, A.; Fuchs, C.; Guida, R.; Gysel, M.; Hansel, A.; Hoyle, C. R.; Jokinen, T.; Junninen, H.; Kangasluoma, J.; Keskinen, H.; Kim, J.; Krapf, M.; Kurten, A.; Laaksonen, A.; Lawler, M.; Leiminger, M.; Mathot, S.; Mohler, O.; Nieminen, T.; Onnela, A.; Petaja, T.; Piel, F. M.; Miettinen, P.; Rissanen, M. P.; Rondo, L.; Sarnela, N.; Schobesberger, S.; Sengupta, K.; Sipilaa, M.; Smith, J. N.; Steiner, G.; Tome, A.; Virtanen, A.; Wagner, A. C.; Weingartner, E.; Wimmer, D.; Winkler, P. M.; Ye, P. L.; Carslaw, K. S.; Curtius, J.; Dommen, J.; Kirkby, J.; Kulmala, M.; Riipinen, I.; Worsnop, D. R.; Donahue, N. M.; Baltensperger, U. The role of low-volatility organic compounds in initial particle growth in the atmosphere. *Nature* **2016**, *533* (7604), 527−531.
(62) Dawson, M. L.; Perraud, V.; Gomez, A.; Arquero, K. D.; Ezell, M. J.; Finlayson-Pitts, B. J. Measurement of gas-phase ammonia and amines in air by collection onto an ion exchange resin and analysis by ion chromatography. *Atmos. Meas. Tech.* **2014**, *7*, 2733−2744.
(63) Ortega, I. K.; Kupiainen, O.; Kurtén, T.; Olenius, T.; Wilkman, O.; McGrath, M. J.; Loukonen, V.; Vehkamäki, H. From quantum chemical formation free energies to evaporation rates. *Atmos. Chem. Phys.* **2012**, *12* (1), 225−235.
(64) McGrath, M. J.; Olenius, T.; Ortega, I. K.; Loukonen, V.; Paasonen, P.; Kurtén, T.; Kulmala, M.; Vehkamäki, H. Atmospheric Cluster Dynamics Code: A flexible method for solution of the birth-death equations. *Atmos. Chem. Phys.* **2012**, *12* (5), 2345−2355.
(65) Vehkamäki, H.; McGrath, M. J.; Kurtén, T.; Julin, J.; Lehtinen, K. E. J.; Kulmala, M. Rethinking the application of the first nucleation theorem to particle formation. *J. Chem. Phys.* **2012**, *136* (9), 094107.
(66) Olenius, T.; Kupiainen-Määttä, O.; Ortega, I. K.; Kurtén, T.; Vehkamäki, H. Free energy barrier in the growth of sulfuric acid-ammonia and sulfuric acid-dimethylamine clusters. *J. Chem. Phys.* **2013**, *139* (8), 084312.
(67) Paasonen, P.; Olenius, T.; Kupiainen, O.; Kurtén, T.; Petäjä, T.; Birmili, W.; Hamed, A.; Hu, M.; Huey, L. G.; Plass-Duelmer, C.; Smith, J. N.; Wiedensohler, A.; Loukonen, V.; McGrath, M. J.; Ortega, I. K.; Laaksonen, A.; Vehkamäki, H.; Kerminen, V. M.; Kulmala, M. On the formation of sulphuric acid - amine clusters in varying atmospheric conditions and its influence on atmospheric new particle formation. *Atmos. Chem. Phys.* **2012**, *12* (19), 9113−9133.
(68) Kürten, A.; Jokinen, T.; Simon, M.; Sipila, M.; Sarnela, N.; Junninen, H.; Adamov, A.; Almeida, J.; Amorim, A.; Bianchi, F.; Breitenlechner, M.; Dommen, J.; Donahue, N. M.; Duplissy, J.; Ehrhart, S.; Flagan, R. C.; Franchin, A.; Hakala, J.; Hansel, A.; Heinritzi, M.; Hutterli, M.; Kangasluoma, J.; Kirkby, J.; Laaksonen, A.; Lehtipalo, K.; Leiminger, M.; Makhmutov, V.; Mathot, S.; Onnela, A.; Petäjä, T.; Praplan, A. P.; Riccobono, F.; Rissanen, M. P.; Rondo, L.; Schobesberger, S.; Seinfeld, J. H.; Steiner, G.; Tomé, A.; Tröstl, J.; Winkler, P. M.; Williamson, C.; Wimmer, D.; Ye, P. L.; Baltensperger, U.; Carslaw, K. S.; Kulmala, M.; Worsnop, D. R.; Curtius, J. Neutral molecular cluster formation of sulfuric acid-dimethylamine observed in real time under atmospheric conditions. *Proc. Natl. Acad. Sci. U. S. A.* **2014**, *111* (42), 15019−15024.

DOI: 10.1021/acs.est.6b04173
Environ. Sci. Technol. 2017, 51, 243−252

(69) Henschel, H.; Kurten, T.; Vehkamaki, H. Computational study on the effect of hydration on new particle formation in the sulfuric acid/ammonia and sulfuric acid/dimethylamine systems. *J. Phys. Chem. A* **2016**, *120* (11), 1886−1896.
(70) Loukonen, V.; Kurtén, T.; Ortega, I. K.; Vehkamäki, H.; Padua, A. A. H.; Sellegri, K.; Kulmala, M. Enhancing effect of dimethylamine in sulfuric acid nucleation in the presence of water - A computational study. *Atmos. Chem. Phys.* **2010**, *10* (10), 4961−4974.
(71) Lana, A.; Bell, T. G.; Simo, R.; Vallina, S. M.; Ballabrera-Poy, J.; Kettle, A. J.; Dachs, J.; Bopp, L.; Saltzman, E. S.; Stefels, J.; Johnson, J. E.; Liss, P. S. An updated climatology of surface dimethlysulfide concentrations and emission fluxes in the global ocean. *Glob. Biogeochem. Cycle* **2011**, *25*, 1.
(72) Ge, X.; Wexler, A. S.; Clegg, S. L. Atmospheric amines − Part I. A review. *Atmos. Environ.* **2011**, *45* (3), 524−546.
(73) Andreae, M. O.; Berresheim, H.; Andreae, T. W.; Kritz, M. A.; Bates, T. S.; Merrill, J. T. Vertical-distribtuion of dimethylsulfide, sulfur-dioxide, aerosol ions, and radon over the northeast Pacific-Ocean. *J. Atmos. Chem.* **1988**, *6* (1−2), 149−173.
(74) Berresheim, H.; Andreae, M. O.; Ayers, G. P.; Gillett, R. W.; Merrill, J. T.; Davis, V. J.; Chameides, W. L. Airborne measurements of dimethylsulfide, sulfur dioxide, and aerosol ions over the Southern Ocean south of Australia. *J. Atmos. Chem.* **1990**, *10* (3), 341−370.
(75) Erisman, J. W.; Vermetten, A. W. M.; Asman, W. A. H.; Waijersijpelaan, A.; Slanina, J. Vertical distribution of gases and aerosols: the behaviour of ammonia and related components in the lower atmosphere. *Atmos. Environ.* **1988**, *22* (6), 1153−1160.
(76) Levine, J. S.; Augustsson, T. R.; Hoell, J. M. The vertical distribution of tropospheric ammonia. *Geophys. Res. Lett.* **1980**, *7* (5), 317−320.
(77) Yu, F.; Luo, G. Modeling of gaseous methylamines in the global atmosphere: Impacts of oxidation and aerosol uptake. *Atmos. Chem. Phys.* **2014**, *14* (22), 12455−12464.
(78) Vanhanen, J.; Mikkila, J.; Lehtipalo, K.; Sipila, M.; Manninen, H. E.; Siivola, E.; Petaja, T.; Kulmala, M. Particle Size Magnifier for Nano-CN Detection. *Aerosol Sci. Technol.* **2011**, *45* (4), 533−542.
(79) Kangasluoma, J.; Kuang, C.; Wimmer, D.; Rissanen, M. P.; Lehtipalo, K.; Ehn, M.; Worsnop, D. R.; Wang, J.; Kulmala, M.; Petäjä, T. Sub-3nm particle size and composition dependent response of a nano-CPC battery. *Atmos. Meas. Tech.* **2014**, *7*, 689−700.

DOI: 10.1021/acs.est.6b04173
Environ. Sci. Technol. 2017, 51, 243−252